Non-Topochemical Reduction of Iron Oxides

S. P. TRUSHENSKI, KUN LI, AND W. O. PHILBROOK

Non-topochemical behavior was studied during reduction of porous spheres of hematite by stages through the intermediate oxides and also continuously to iron by CO/CO_2 mixtures at temperatures of 600 to 900°C (873 to 1173 K). The behavior became more nearly topochemical as temperature increased. Shrinking occurred during the reduction of hematite to magnetite and of magnetite to wüstite, whereas swelling was observed during the reduction of wüstite to iron. Shrinking was greater, and swelling less, at higher temperatures. The total surface area of the solid decreased with increasing extent of reduction during each of the three stages. A non-topochemical model was developed which satisfies, better than previously proposed models, the reduction data for the single reactions and the three reactions occurring simultaneously. The model provides for variation in particle size and local changes in porosity and effective diffusivity. An empirical "sintering exponent" was introduced to describe changes in reacting surface area.

SEVERAL mathematical models have been proposed in the literature to explain numerous results obtained in the study of the reduction of iron oxides. Although a specific model may explain one set of data, it will seldom satisfy other sets. Not only do reported rate constants differ by orders of magnitude, but the activation energies also vary over a wide range.

These contradictions can be partially explained by the wide diversity of experimental conditions and starting materials used by various investigators. Some of the conflicting observations have been clarified by Spitzer *et al.*[1-3] who developed several models to explain the topochemical reduction of iron oxides at one, two or three advancing interfaces. However, topochemical reaction, although usually observed during the reduction of dense particles of iron oxides, is not the general behavior. In porous particles the interfaces become diffuse as porosity increases until no distinguishable interface is observable between successive solid phases. This non-topochemical behavior is not so well analyzed in the literature, but it is illustrated by some reports on the reduction of porous particles.

Ahner and Feinman[4] studied the reduction of Venezuelan ore with hydrogen and found that the rate was independent of particle size. Micrographic examination showed that no oxygen gradients existed within a particle and that larger grains were in the same state of reduction as smaller ones. However, it was observed that individual grains within the particle reduced topochemically. Helfrich and Sollenberger[5] made similar observations. These are examples of homogeneous reduction on the macroscopic scale and topochemical reaction on the microscopic scale.

Reduction behavior is also a function of temperature. Hansen *et al.*[6] observed non-topochemical reduction when hematite was reduced to magnetite at 430°C with $CO-CO_2$ mixtures. Edström[7,8] noted the reduction of sintered particles of hematite to magnetite with carbon monoxide to be topochemical at 800°C but non-topochemical at 427°C. Based on a detailed study of hydrogen reduction of natural and synthetic hematite, Turkdogan and Vinters[9] concluded that the rate processes involved are far more complex than those realized by previous investigators. Depending on the temperature, particle size and porosity, and the level of reduction, three basic rate processes—uniform internal reduction, limiting mixed control (diffusion in the pores and reaction on pore walls), and gas diffusion in reduced iron layer, may control the rate of reduction individually or collectively.

Since a topochemical model does not accurately describe reduction in porous particles or at low temperatures, efforts have been made by several workers to develop more comprehensive models.

Bowen and Cheng[10] proposed a model which allows reaction to take place in a narrow zone of arbitrary width over which the concentration gradient is assumed constant. No analysis was made of any experimental data. Ishida and Wen[11,12] developed a generalized model which reduces to a topochemical model when diffusion is controlling and to homogeneous reaction when chemical kinetics is controlling. Their model was restricted to a single, isothermal, first-order, irreversible reaction with quasi-steady state for the gas phase and particles of constant size, porosity, and effective diffusivity.

Szekely and Evans[13,14] formulated a non-topochemical model by assuming that a porous particle consists of numerous dense spherical subparticles of identical size which react topochemically on a microscopic scale. This model, limited to a single reaction occurring in a particle of constant size with dense spherical subparticles of unchanging size, was successfully applied to the reduction of nickel oxide with hydrogen below 620°C. Above 620°C, this model predicted reduction rates much greater than observed.

From predictions of models such as those just outlined it is observed that topochemical reaction occurs in a porous particle only if diffusion controls the rate of each reaction. (The unreacted core of a theoretically dense particle may recede topochemically if chemical kinetics at the interface controls the rate of reaction to form a shell of porous product.) If the rate of an individual chemical reaction becomes comparable to that of transport through the porous solid, then reaction will occur throughout a finite volume rather than

S. P. TRUSHENSKI is Senior Research Engineer, Amoco Production Co., Tulsa, Okla. KUN LI and W. O. PHILBROOK are Professor of Chemical Engineering and Professor of Metallurgy and Materials Science, respectively, Carnegie-Mellon University, Pittsburgh, Pa. 15213.

Manuscript submitted June 7, 1973.

at an interface, and topochemical behavior will no longer be observed macroscopically.

The non-topochemical models that have been developed thus far make no allowance for changes in either local properties or gross dimensions of the particles arising from shrinking, swelling, sintering, or other changes during the reaction, and hence do not accurately describe the process in detail. The objective of this study was to measure changes in particle properties during reduction of porous hematite by CO by stages and overall, and to describe these observations by a mathematical model to predict the non-topochemical reduction of porous hematite pellets.

THEORY

The particular reaction system under study is the set of consecutive reactions:

$$3Fe_2O_3 + CO \underset{k_{-1}}{\overset{k_1}{\rightleftharpoons}} 2Fe_3O_4 + CO_2 \qquad [1]$$

$$\frac{x}{4x-3} Fe_3O_4 + CO \underset{k_{-2}}{\overset{k_2}{\rightleftharpoons}} \frac{3}{4x-3} Fe_xO + CO_2 \qquad [2]$$

$$Fe_xO + CO \underset{k_{-3}}{\overset{k_3}{\rightleftharpoons}} x\,Fe + CO_2 \qquad [3]$$

For a differential volume element in the particle, the equation of continuity for a species in the gas phase is

$$\frac{\partial c_i \epsilon}{\partial t} + \nabla \cdot \epsilon c_i v^* - \nabla \cdot D_i \nabla c_i = R'_i \qquad [4]$$

The reactions described by Eqs. [1] to [3] are equimolar in the gas phase, and it is usually concluded that v^* is zero. This is not precisely true when the void fraction of the solid is a function of position and time. However, the total volume of gas entering and leaving the particle is so large compared with the void volume and dimensional changes, that the accumulation and net convection terms are negligibly small compared with the diffusion and reaction terms. Hence, Eq. [4] may be simplified to:

$$-\nabla \cdot D_i \nabla c_i = R'_i \qquad [5]$$

Neglecting diffusion, the equation of continuity for a solid species may be written

$$\frac{\partial c'_i}{\partial t} + \nabla \cdot c'_j u = R'_j \qquad [6]$$

where u is the velocity of the solid, which, in the absence of diffusion, is identical to the molar average velocity of the solid and also to the velocity of each species. The convection term in Eq. [6] is not always negligible, especially when large volume changes occur during reduction.

A relatively simple technique was used to include the convection of solids in the numerical solution. This technique basically assumes that the convective effect is negligible in each radial increment, Δr, during a time increment Δt. After reduction has occurred for this Δt, new calculations are made of solid composition. It is assumed that shrinking and swelling are a function of composition alone, so after each time increment a new radial increment is determined. This radial increment will contain the same number of iron atoms as it initially did but the width will depend on the local composition. Thus, the system is solved numerically as a series of batch reactors of changing size and composition while a constant mass balance is always maintained on the iron atoms. It is also assumed for these calculations that the composition is uniform over the radial increment.

If it is assumed that the spherical particle is initially homogeneous and that only radial gradients in the gas- and solid-phase concentrations exist, Eq. [5] for CO in an ideal gas mixture at constant pressure becomes

$$-D_{CO}\left(\frac{d^2 p_{CO}}{dr^2} + \frac{2}{r}\frac{dp_{CO}}{dr}\right) - \left(\frac{dD_{CO}}{dr}\frac{dp_{CO}}{dr}\right) = (RT)R'_{CO}$$
$$0 < r < r_0 \qquad [7]$$

and Eq. [6]:

$$\frac{\partial c'_j}{\partial t} + \frac{1}{r^2}\frac{\partial}{\partial r}(r^2 c'_j u) = R'_j, \qquad 0 < r < r_0 \qquad [8]$$

These equations are subject to the initial and boundary conditions:

For the reactant gas phase:

$$D_{CO}\frac{dp_{CO}}{dr} = k_G(p^b_{CO} - p_{CO}), \quad \text{at } r = r_0 \qquad [9]$$

$$\frac{dp_{CO}}{dr} = 0, \quad \text{at } r = 0 \qquad [10]$$

For the solid phase:

$$c'_j = c^0_j, \qquad t = 0 \qquad [11]$$

$$u = 0, \qquad \text{at } r = 0 \qquad [12]$$

The mass transfer coefficient, k_G, can be determined by the correlation of Ranz.[15]

It will be assumed that the hematite-magnetite reaction is irreversible and first-order and that both the magnetite-wüstite and wüstite-iron reactions are reversible and first order with respect to the gas. In addition, the reduction rate is assumed to be directly proportional to the specific interfacial area *i.e.*, area available for reaction per unit volume of particle. From Eqs. [1] to [3], the rates of reactions producing the various solid species are given by

$$R'_h = \frac{-3k_1}{RT}(S_h p_{CO}) \qquad [13]$$

$$R'_m = \frac{1}{RT}\left\{2k_1 S_h p_{CO} - \frac{xk_2}{4x-3} \times S_m[(1 + 1/K_2)p_{CO} - p/K_2]\right\}, \qquad [14]$$

$$R'_w = \frac{1}{RT}\left\{\frac{3}{4x-3}k_2 S_m[(1 + 1/K_2)p_{CO} - p/K_2] - k_3 S_w[(1 + 1/K_3)p_{CO} - p/K_3]\right\}, \qquad [15]$$

$$R'_{Fe} = \frac{1}{RT}\left\{xk_3 S_w[(1 + 1/K_3)p_{CO} - p/K_3]\right\}, \qquad [16]$$

and of CO by:

$$R'_{CO} = \frac{1}{RT}\left\{-k_1 S_h p_{CO} - k_2 S_m[1 + 1/K_2)p_{CO} - p/K_2] - k_3 S_w[(1 + 1/K_3)p_{CO} - p/K_3]\right\} \qquad [17]$$

where K_2 and K_3 are equilibrium constants and equal to k_2/k_{-2} and k_3/k_{-3} respectively.

Solution of the coupled Eqs. [7] and [8] with the reacting surface areas, S_j, and the effective diffusivity, D_{CO}, being functions of position, composition and possibly time, and u a function of local composition, is possible only by numerical methods.

Before such a numerical solution can be obtained, relationships among particle size, local void fraction, reacting surface area and local composition must be determined. It was found experimentally that the overall particle size was primarily a function of composition and secondarily influenced by reduction time. In all calculations it has been assumed that the overall particle size is a function of composition alone.

When a 60 pct reduced hematite particle was sectioned, it was noted that the porosity near the surface was very high while the center was quite dense. It was also found that the iron concentration was high at the surface while the wüstite concentration was high at the center. This indicated that shrinking and swelling were functions of local composition. Thus it is conceivable that the particle was simultaneously expanding at its exterior where iron was being produced and shrinking in the interior where wüstite was forming.

The local void fraction within the particle may vary as a result of two phenomena: differences in theoretical volume for hematite, magnetite, wüstite, and iron (15.24, 14.9, 12.75, 7.10 cm^3/g-at Fe, respectively), and shrinking or swelling of the solid during reduction. Variations of the local void fraction result in variations of the effective diffusivity, D_{CO}. The relationship between the effective diffusivity and porosity may be represented by the simplified form of an equation developed by Newby[16] for a random system of identical spheres.

$$D_{CO} = \mathfrak{D}_{CO\text{-}CO_2} 0.5\epsilon (1 + \epsilon). \qquad [18]$$

The local void fraction is not readily measured experimentally but will be assumed to vary only with local composition in exactly the same manner as the average void fraction varies with the average particle composition.

Since the effective diffusivity is a function of void fraction which varies with local composition, the term $-\left(\frac{dD_{CO}}{dr}\frac{dp_{CO}}{dr}\right)$ of Eq. [7] is not zero as is often assumed in other models. It was found that if this term was neglected, errors of up to 16 pct in the mass balance could be introduced when moles of CO transported were compared to moles of oxide reacted.

Not directly measurable, the specific reacting surface area for each of the three reduction reactions can only be estimated. If it is assumed[13] that a porous pellet consists of dense, spherical grains of uniform and unchanging size and that each grain reacts topochemically, the reacting surface area of the grain can be shown to decrease as the two-thirds power of the fraction of the unreacted solid. The BET surface area of a porous hematite pellet was equivalent to a mean grain radius of 5.7×10^{-6} cm computed using the above assumption. In comparison, magnetite reduced from the same hematite at 750°C had a measured surface area corresponding to a mean radius of 13.6×10^{-6} cm. This reflects considerable local sintering and invalidates the assumption of constant grain size. However, it seems reasonable that the local reacting surface area for each reaction varies as some function of local composition only. On a purely empirical basis, the function is assumed to be of an exponential form.

Thus, for the reactions of interest:

$$S_h = S_h^0 X_h^a \qquad [19]$$

$$S_m = S_m^0 X_m^b \qquad [20]$$

$$S_w = S_w^0 X_w^c \qquad [21]$$

where X_h, X_m and X_w are the dimensionless concentrations of hematite, magnetite and wüstite, respectively, defined as the fraction of the local concentration of iron atoms that appears in the designated species. The exponents a, b, and c are empirical constants which are determined by variation until a best fit with experimental data is obtained. These exponents will be called the *sintering exponents*. The specific surface area of hematite, magnetite and wüstite (S_h^0, S_m^0, S_w^0) must be determined experimentally for a typical particle under study.

EXPERIMENTAL WORK

A thermogravimetric method was used to follow the kinetics of the reduction. A spherical particle was suspended from a Ni-span C spring balance into an alumina reaction tube heated by a molybdenum-wound resistance furnace. A spring constant of 2.802 cm/g was determined, and spring displacements were followed with a cathetometer capable of reading to within 0.005 cm. Furnace temperatures were controlled to ±2°C.

Preliminary runs were made to observe the variation of reduction behavior with temperature, gas composition, particle size and porosity. Most samples were *green* (unsintered) spheres, made from 99.9 pct pure hematite powder, with an initial weight of approximately 2 g and diameter of 1.35 cm. It was found that the degree of non-topochemical reduction decreased as temperature increased. Catastrophic swelling occurred at 900°C in highly porous as well as dense particles. At higher temperatures (900°C) the reduction rate decreased as initial particle density increased while at lower temperatures (650 to 800°C) the reduction rate appeared to be independent of the initial particle void fraction in the range of 0.45 to 0.78. For very dense particles ($\epsilon^0 \cong 0$) the reduction rate was significantly decreased by decreasing the initial void fraction. Generally, *green* porous particles shrank during magnetite and wüstite production, although further sintering might not occur during the reduction of presintered particles. Carbon deposition rates in the range 600 to 700°C were significant, necessitating the use of reducing-gas compositions that would not deposit carbon.

A set of experimental runs was made to show that the non-topochemical model could be used to fit or predict actual reaction rates. Three temperatures were investigated: 750, 775, and 800°C. The reactions of hematite to magnetite and magnetite to wüstite were each studied independently so that rate constants and activation energies could be established for these reactions without their being masked by the wüstite-iron reation. This was done by controlling the gas compo-

sition carefully so that an oxide initially present could react only to the next lower one. Another set of runs was made at bulk gas compositions capable of reducing hematite to iron, so reactions [1] to [3] occurred consecutively and the rate constant of each of these three reactions was determined. For all of the runs the initial hematite particle had a diameter of 1.35 cm and was not presintered. The hematite particles had initial weights of approximately 2 g (±0.4 g) and initial void fractions of $\epsilon^0 \cong 0.75$ (±0.07). In general, the gas flow rate through the reactor was low with a particle Reynolds number of approximately 4.

Three important physical parameters were measured during the reactions. First, the change in particle size was measured as a function of reduction by stopping the reaction at various stages, removing the particle and measuring its diameter. The change in total surface area was also measured at various degrees of reduction. The particle sizes were used to predict local void fractions and the surface area to define the initial specific surface area of each species and to identify microscopic sintering. Finally, the particle weight was measured as a function of time during reduction.

CORRELATION OF PARTICLE CHARACTERISTICS

In all runs for the reduction of hematite to magnetite, the particle size decreased as conversion increased. In general, the longer the reduction time (also the higher the conversion), the greater the extent of sintering. Since relatively small volume change occurred (~16 pct) when hematite was reduced to magnetite, the void fraction of the particle did not change appreciably (from 0.71 to 0.65). For this reason it has been assumed that during the reduction of hematite to magnetite the particle radius is a linear function of the average fraction of magnetite,

$$r_0 = r_0^0 - (r_0^0 - r_0^\infty)\,\overline{X}_m \qquad [22]$$

where r_0^0 and r_0^∞ are initial and final radii of the particle.

It was assumed earlier that the local void fraction, ϵ, is described by the same equation as the average void fraction, except that the local composition is substituted for the average composition. Therefore the local void fraction at any point within the particle is given by

$$\epsilon = 1 - \frac{\left[\dfrac{m^0(1 - 0.0334X_m)}{(4/3)\,\pi\,(r_0^0 X_h + r_0^\infty X_m)^3}\right]}{\left[\dfrac{3X_hM_h + 2X_mM_m}{\dfrac{3X_hM_h}{\rho_h} + \dfrac{2X_mM_m}{\rho_m}}\right]} \qquad [23]$$

Similar studies were made for the reduction to wüstite of magnetite prepared from hematite. Generally, the degree of sintering increased as the fractional reduction increased. The volume change was quite significant. For example, at 750°C the volume of a particle decreased 49 pct during the reduction. This represents an average void fraction decrease of 40 pct (from 0.640 to 0.381). It is, therefore, important that the particle size as a function of conversion be represented more accurately than for reduction of hematite to magnetite. The data indicates that the particle radius can be represented by an empirical equation of the form

$$r_0 = r_0^0 - (r_0^0 - r_0^\infty)\,\overline{X}_w^q \qquad [24]$$

where q was determined to have a value of 6.15 at 750°C, 2.30 at 775°C and 2.66 at 800°C. The local void fraction of the particle was described by an equation similar to [23].

In the consecutive reduction of hematite to iron, the particles sintered very rapidly during the initial stages of reduction. This sintering continued until approximately 30 pct reduction. Above 30 pct reduction the particle began to swell to varying degrees. The minimum particle size decreased as temperature increased, reflecting the effect of temperature on sintering. The particles swelled more at 750°C than at 775°C or 800°C. This may be explained if the change in particle size is thought of as a result of simultaneous shrinking due to sintering and swelling caused by chemical effects. As no swelling was observed during the reduction of hematite to magnetite and magnetite to wüstite, it was concluded that the swelling was a result of the wüstite-to-iron reaction rather than being caused by purely physical forces.

When particles were sectioned at various stages of reduction only hematite and magnetite were observed up to 10 pct reduction. At 30 pct reduction a small amount of iron was observed near the surface with the remainder being magnetite and wüstite. Above 50 pct reduction only wüstite and iron were observed. This indicated that the reduction was essentially step-wise.

The particle size was related to the average particle composition by the empirical equation:

$$r_0 = \overline{X}_h r_h^0 + \overline{X}_m r_m^0 + \overline{X}_w r_m^0 + \overline{X}_{Fe} r_{Fe}^0 + (r_w^0 - r_m^0)\,\overline{X}_w^q \qquad [25]$$

For the initial samples used in these studies, the values of r_j^0 determined from the experimental data were:

Temperature	r_h^0, cm	r_m^0	r_w^0	r_{Fe}^0
(1023 K) 750°C	0.675	0.635	0.478	0.625
(1048 K) 775°C	0.675	0.653	0.496	0.517
(1073 K) 800°C	0.675	0.615	0.470	0.502

Table I. Total Surface Area During Reduction of Hematite to Magnetite

Run Number	(K)	Temp., °C	Initial Wt (g)	Fractional Reduction*	Surface Area (m^2/g)
64	Ambient	–	1.6183	0.000	9.98
65		–	1.8524	0.000	10.10
66		–	2.1000	0.000	10.22
67		–	2.3363	0.000	10.59
177		–	1.8865	0.000	9.78
178			2.2960	0.000	10.03
88	1023	750	1.9835	0.627	5.83
87		750	2.1587	0.932	4.36
144	1048	775	2.4711	0.965	3.07
146		775	2.0047	0.959	3.23
112	1073	800	2.1265	0.997	3.42
115		800	2.2505	0.939	2.96

*Fraction of Fe or O atoms initially in hematite as magnetite.

Satisfactory representation by Eq. [25] of the experimentally observed change of particle size was obtained with q = 2.15 at 750°C and 1.00 at 775°C and 800°C. The local void fraction at any point within the particle was calculated as:

$$\epsilon = 1 - \frac{\left[\dfrac{m^0(1 - 0.3006\,X_{Fe} - 0.0893\,X_w - 0.0334\,X_m)}{(4/3)\,\pi\,(X_h r_h^0 + X_m r_m^0 + X_w r_m^0 + X_{Fe} r_{Fe}^0 + (r_w^0 - r_m^0)\,X_w^q)^3}\right]}{\left[\dfrac{\dfrac{X_h M_h}{2} + \dfrac{X_m M_m}{3} + \dfrac{X_w M_w}{x} + \dfrac{X_{Fe} M_{Fe}}{1}}{\dfrac{X_h M_h}{2\rho_h} + \dfrac{X_m M_m}{3\rho_m} + \dfrac{X_w M_w}{x\rho_w} + \dfrac{X_{Fe} M_{Fe}}{\rho_{Fe}}}\right]} \qquad [26]$$

Total surface area measurements were made with a B.E.T. apparatus. Table I lists the measured area of hematite undergoing reduction to magnetite. For unreacted samples the total surface area per unit mass was essentially uniform at 10 m^2/g. Significant decreases in area occurred when hematite was reduced to magnetite, the change being greater at higher temperatures. The decrease in area was the result of several phenomena. Probably among the most important were the sintering of grains and the closing of pores. As average grain size increased by recrystallization and growth, the area exposed to gas was decreased. Similarly, if pore necks closed, the pores thus encapsulated were no longer available as effective surface or diffusion pathways.

Similar measurements of surface area were made during reduction of magnetite to wüstite. Once again, the area decreased as the conversion increased and the extent of decrease increased with increasing temperature.

The specific surface area per unit volume of particle was computed from experimentally determined values of surface area per unit mass of pure component as follows:

$$S_j^0 = 10^4\, s_j^0\, m^0/[(4/3)\,\pi\,(r_j^0)^3], \quad cm^{-1} \qquad [27]$$

The values of s_j^0 used were:

	(1023 K) 750°C	(1048 K) 775°C	(1073 K) 800°C
s_h^0	10.0 m^2/g	10.0	10.0
s_m^0	4.25	3.23	2.96
s_w^0	1.50	0.95	0.65

Area measurements were also made on particles of hematite which had been partially reduced to iron. These measurements are listed in Table II. Total surface area decreased as the fractional reduction increased. The overall changes were by factors of 30 at 750°C, 40 at 775°C, and 50 at 800°C. It was shown previously that during reduction a particle initially shrinks and then begins to swell above 30 pct reduction. Yet surface area continues to decrease during the entire reduction period.

It thus appears that on the microscopic scale the grains continue to grow causing a decrease in surface area, while the pore volume increases as iron begins to form as a result of the whisker-like growth of iron filaments. Sintering from purely physical effects is usually characterized by both grain growth and concurrent decrease in pore volume, with a resultant decrease in macroscopic particle size. However, when sintering occurs as a result of chemical reaction, the continuing coalescence of grains and decrease of surface area are not necessarily accompanied by a decrease in pore volume.

The sintering exponents a, b and c are, in a way, a measure of the degree of sintering during reduction. A higher value of the exponent indicates more extensive loss of surface area by sintering.

Table II. Total Surface Area During Reduction of Hematite-to Iron

Run Number	(K)	Temp, °C	Initial Wt (g)	Fractional Reduction*	Surface Area (m^2/g)
67	1023	750	2.3363	0.000	10.59
77		750	2.0515	0.134	4.75
78		750	2.0199	0.206	3.39
79		750	2.0061	0.297	1.84
80		750	1.9615	0.407	1.53
81		750	1.9053	0.509	1.18
82		750	1.9117	0.605	1.34
83		750	2.1676	0.699	1.01
84		750	1.9480	0.806	0.51
85		750	1.9566	0.899	0.45
86		750	1.8437	0.984	0.37
67	1048	775	2.3363	0.000	10.59
168		775	2.2972	0.112	4.84
166		775	2.0129	0.307	1.21
174		775	2.1278	0.804	0.32
169		775	2.1434	0.967	0.26
170		775	2.0699	0.960	0.32
67	1073	800	2.3363	0.000	10.59
135		800	2.1675	0.117	3.97
133		800	2.3273	0.327	0.46
138		800	2.1444	0.724	0.28
139		800	2.0225	0.991	0.20
140		800	2.0031	0.988	0.21

*Fraction of 0 atoms initially in hematite that have been removed.

EVALUATION OF MODEL

Fig. 1 shows a typical fit of the model to the experimental data for the reduction of hematite to magnetite at 775°C. The model was fitted to the experimental data by adjusting the rate constant and sintering exponent until agreement was judged satisfactory by visual inspection. No attempt was made to adjust these constants so that a given confidence factor would be satisfied because of the excessive computer time required. Generally, the effect of k_1 on the predicted fractional reduction was to influence the initial stages of reac-

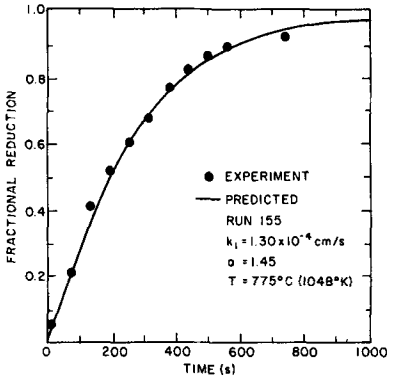

Fig. 1—Comparison of model with experimental data for reduction of hematite to magnetite at 775°C, 14.1 pct CO.

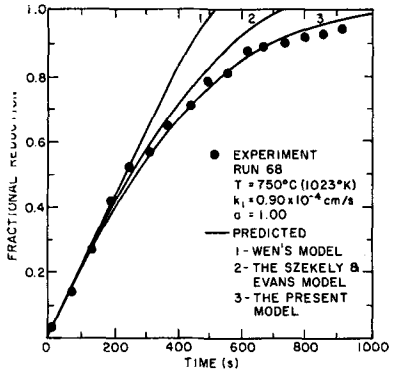

Fig. 2—Comparison of the present non-topochemical model with Wen's and Szekely and Evans' models. Reduction of hematite to magnetite at 750°C, 10.70 pct CO, r_0^0 = 0.675 cm, ϵ^0 = 0.71.

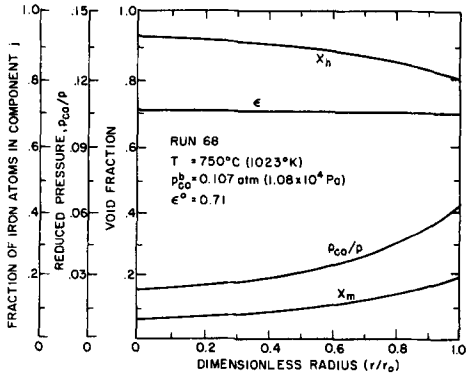

Fig. 3—Predicted profiles of void fraction, gas and solid compositions within the particle after 70 s during reduction of hematite to magnetite.

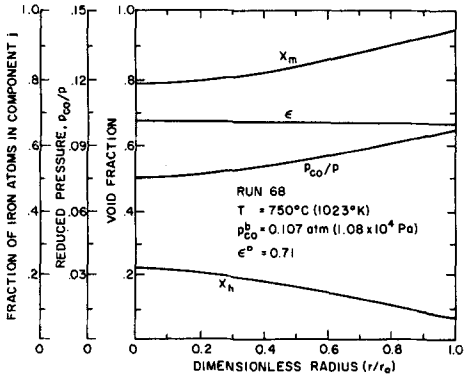

Fig. 4—Predicted profiles of void fraction, gas and solid compositions within the particle after 670 s during reduction of hematite to magnetite.

tion while the sintering exponent, a, influenced the reaction rate at later stages.

Fig. 2 is a plot of Wen's[17] and Szekely and Evans'[13,14] models and the present non-topochemical one for run 68 at 750°C. Wen's model fits the data initially but predicts that the reaction rate would continue to be rapid until 90 pct conversion and then decrease with depletion of the reactant solid at the surface. Szekely and Evans' model fits the data somewhat better than Wen's but not as well as the present model. It may be concluded that the effects of solid composition and sintering must be included in the mathematical description of the reduction of porous particles of iron oxide.

Predicted profiles of void fraction, and solid and gas compositions within the particle at 70 and 670 s are shown in Figs. 3 and 4. No experimental data have been obtained on local compositions within the particle, but qualitative observations support the predicted trends. The model predicts that reaction continues throughout the entire particle; the extent depends on the relative diffusive and chemical resistances. The reaction is neither topochemical nor homogeneous.

Fig. 3 shows concentration profiles after 70 s when the reaction rate is fast near the particle surface and slows gradually towards the center. It is of interest to note that the drop in CO concentration from the bulk stream to the particle surface (10.7 to 6.39 pct) is nearly as large as the drop from the particle surface to its center (6.39 to 2.34 pct).

Fig. 4 shows profiles after 670 s when the major portion of the reaction is now occurring near the center rather than near the surface of the particle. Although the reactant gas concentration is higher near the surface than at the center, the rate of reaction is slower near the surface because of a smaller specific reacting surface.

A typical fit of the model to experimental data for the reduction of magnetite to wüstite at 800°C is shown in Fig. 5. All magnetite particles used in these studies were prepared from *green* hematite particles. In the model it was assumed that the magnetite particle was initially uniform in porosity and specific surface.

As in the case of the hematite-to-magnetite reaction, the rate constant, k_2, influences the initial reaction rate primarily, while the sintering exponent, b, influences the later stages of reaction. Both k_2 and b are adjustable parameters which were varied until a satisfactory fit was obtained. During the reduction of magnetite to wüstite, shrinkage was observed. The degree of shrink-

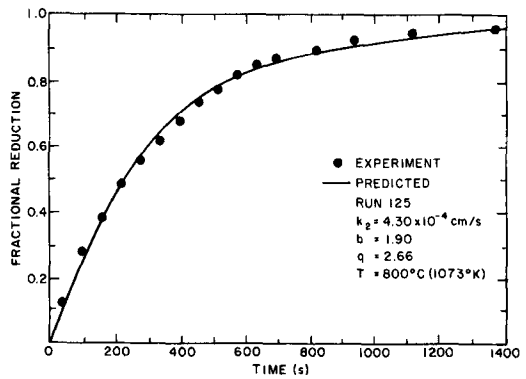

Fig. 5—Comparison of model with experimental data for reduction of magnetite to wüstite at 800°C, 49.11 pct CO, r_0^0 = 0.635 cm, ϵ^0 = 0.59.

age increased as temperature increased. Similarly, the rate of decrease of surface area increased as temperature increased.

Radial profiles predicted by the model were similar to those shown in Figs. 3 and 4 for the hematite-magnetite reaction except that the gradients in local void fraction were greater as a result of more extensive sintering during the reaction.

Fig. 6 shows a typical fit of the model incorporating three consecutive reactions to experimental data for the reduction of hematite to iron at 775°C. The fits were generally better than those for the hematite-to-magnetite and magnetite-to-wüstite reactions. This may be expected since only two parameters were adjusted for the single reactions while six parameters, two for each reaction, could be varied to obtain a good fit for the reduction of hematite to iron. However, as will be shown, adjusting six parameters to one set of data is not as questionable as it may first appear to be.

At all three temperatures, the data exhibited similar characteristics. Initially, the reaction rate was very high, but above 20 pct reduction an abrupt change occurred. Between 20 and 30 pct reduction, the rate decreased dramatically, indicating a change in either the mechanism that controlled the reaction rate or the predominant reaction. Above 30 pct reduction, the rate was essentially constant or gradually decreasing. If the three reduction reactions were step-wise and uniform throughout the particle, the entire particle would be converted to magnetite after approximately 10 pct reduction and to wüstite after 30 pct reduction. Since the change in reaction rate occurred between 20 and 30 pct reduction, it is inferred that the dominant reaction was changing from magnetite-to-wüstite to wüstite-to-iron.

When partially reduced particles were sectioned it was observed that at 8 pct reduction, hematite and magnetite were the only visible components in the particle. At 20 pct reduction neither hematite nor iron was visible, but wüstite and magnetite were observed. At 30 pct reduction, iron was present near the surface of the particle, and the structure was primarily wüstite with some magnetite at the center. Above 30 pct reduction, the amount of magnetite decreased continually until none was evident at 50 pct reduction. Above 50 pct reduction, only wüstite and iron were present.

It may, therefore, be concluded that at low CO concentrations (about 72 pct CO) in the inlet gas the reduction is nearly step-wise; *i.e.*, hematite-to-magnetite is the main reaction initially, the magnetite-to-wüstite reaction dominates the intermediate stages, and finally the wüstite-to-iron reaction gains ascendancy.

If the model predicts the observed behavior, then variations in k_1 and a should only affect the first 10 pct of reduction; changes in k_2 and b should influence the reduction rate primarily in the range from 10 to 30 pct reduction; and k_3 and c should affect the predictions above 30 pct reduction. For this reason, adjusting all these parameters to fit the data is not as arbitrary as it might seem.

Fig. 7, a plot of predicted average particle composition as a function of time for Run 105 at 750°C, shows that the hematite particle begins to react very fast initially to form magnetite. After approximately 300 s all hematite has been reduced to magnetite. The rate of conversion of hematite to magnetite is nearly constant during the first 200 s of reduction.

The concentration of magnetite increases sharply to about 65 pct at 85 s and then begins to decrease. The decrease is rapid initially and then slows after 500 s. Since the magnetite concentration does not reach 100 pct, the reduction is not truly step-wise, but the rapid increase and then decrease in concentration gives a step-wise appearance.

The model predicts a time lag of approximately 20 s before any wüstite is formed. This is because no wüstite can form until the CO concentration at the particle surface reaches 32 pct, which does not occur until 25 s of reduction time has elapsed. Once wüstite begins to form, its concentration increases rapidly and then decreases at an almost constant rate. From Fig. 7 it is apparent that the reduction of magnetite to wüstite is nearly step-wise since the concentration of wüstite reaches a maximum of 90 pct before decreasing. At the point of maximum $\overline{X}_W$, which occurs at 625 s, little magnetite (6 pct) and iron (4 pct) are present. No iron forms until all the hematite has been converted to magnetite, which occurs at about 325 s. This coincides with the time when the gas at the particle surface becomes rich enough in CO to reduce wüstite to iron. The rate of production of iron is much slower than that of magnetite or wüstite. This is the result of several factors. First, the reacting surface area is much less for the reduction of wüstite than for the higher oxides because of sintering and agglomeration of grains. Second, at a given CO concentration, the thermodynamic driving force is much less for the production of iron than for wüstite or magnetite.

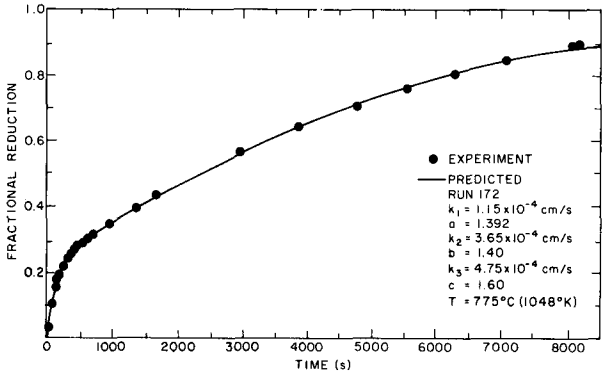

Fig. 6—Comparison of model and experimental data for reduction of hematite to iron at 775°C, 72.38 pct CO, r_0^0 = 0.675 cm, ϵ^0 = 0.655.

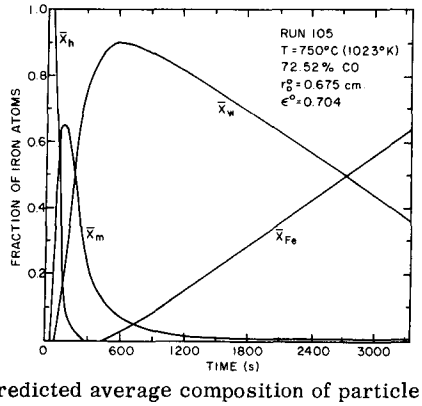

Fig. 7—Predicted average composition of particle as a function of time.

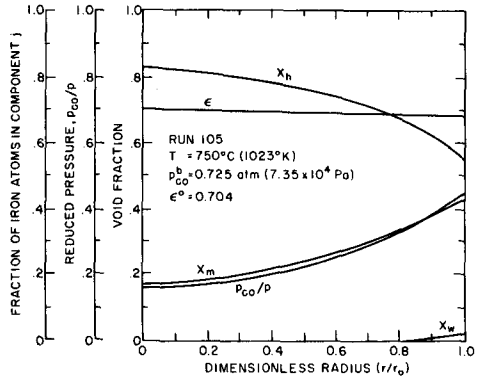

Fig. 8—Predicted profiles of void fraction, gas and solid compositions within the particle after 25 s during reduction of hematite to iron.

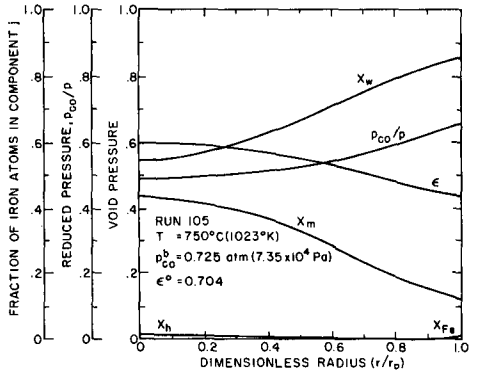

Fig. 9—Predicted profiles of void fraction, gas and solid compositions within the particle after 325 s during reduction of hematite to iron.

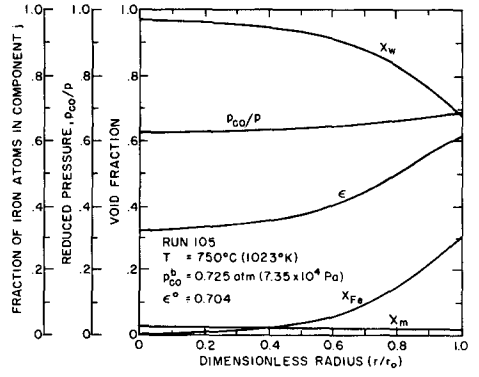

Fig. 10—Predicted profiles of void fraction, gas and solid compositions within the particle after 1105 s during reduction of hematite to iron.

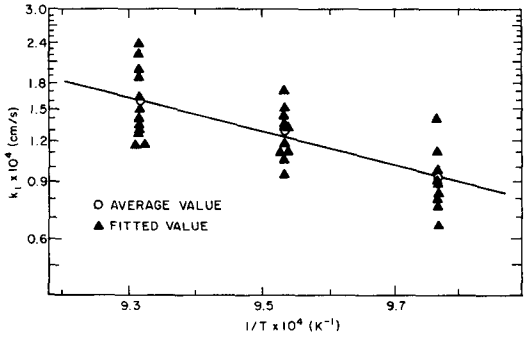

Fig. 11—Arrhenius plot of rate constants for the single reaction of hematite to magnetite.

Figs. 8 to 10 show the predicted radial profiles of gas and solid concentrations and void fraction for Run 105 after 25, 325, and 1105 s, respectively. After 25 s of reduction, no iron is present in the particle and wüstite is just beginning to form at the particle surface. The gas composition is such that wüstite can be formed only in the outer 25 pct of the particle radius. The magnetite concentration profile is practically the mirror image of the hematite concentration profile since no iron is present and X_w is quite small. The void fraction is fairly constant across the entire particle.

After 325 s (Fig. 9), practically all of the hematite has reacted to form magnetite. Iron has just begun to form at the surface of the particle, because the CO concentration of 65 pct at the particle surface slightly exceeds the equilibrium concentration of 62.5 pct for the wüstite-iron reaction.

At this stage of reduction (25.4 pct) it is quite evident that the predominant reaction is the conversion of magnetite to wüstite. The void fraction changes considerably across the particle. The average particle void fraction has decreased from 0.70 to 0.50 and the particle radius from 0.675 to 0.544 cm. Because of considerable sintering occurring during wüstite formation and a higher wüstite concentration at the particle surface than at the center, the void fraction at the particle surface is significantly less than that at the center.

Fig. 10 shows no hematite and very little magnetite remaining after 1105 s. The major reaction now is the reduction of wüstite to iron and reduction is still non-topochemical. (Although the diffusional resistance is increasing relative to the chemical resistance.) Since the overall reaction rate has decreased significantly, the CO concentration gradient is no longer as large as shown in Figs. 8 and 9.

It is interesting to note that the gradient in the void fraction has reversed. The increase in void fraction near the particle surface is the result of swelling when iron is produced. Since the model assumes that swelling increases with increasing iron concentration, the void fraction profile approximately parallels the iron concentration profile.

For each of the three-reaction systems studied (hematite-magnetite, magnetite-wüstite, hematite-magnetite-wüstite-iron) several experimental runs were made at each of the three temperatures (750, 775, and 800°C). This was done in order to obtain more reliable average values of rate constants and sintering exponents.

For the reduction of hematite to magnetite and of magnetite to wüstite, the values of the rate constants and sintering exponents were determined individually for each run. Fig. 11 shows an Arrhenius plot of k_1 for the hematite-to-magnetite reaction. Although not highly reproducible, the individual values at each temperature vary no more than 50 pct from the average. The average values fall closely on a straight line. As to the value of a, they vary within 30 pct of the average at each temperature. Very similar variations were noted in k_2 and b for the magnetite-to-wüstite reaction. The activation energy was determined from the straight line drawn through the average values of k_2 at each temperature. Table III lists the average values of rate constants, sintering exponents and ac-

tivation energies, including those deduced from the data for the reduction of hematite to iron.

In fitting the model to the data for the reduction of hematite to iron, six constants must be adjusted: k_1, a; k_2, b; k_3 and c. The value of a used at each temperature was the average for the single hematite-magnetite reaction. It has been mentioned previously that the reduction of hematite to iron occurs nearly stepwise and consequently the adjustment of these parameters is somewhat restrictive.

It might be pointed out that if the gas flow rate were increased to such a point that the CO concentrations at the particle surface and in the bulk gas were nearly identical, wüstite and iron would be produced almost instantaneously. If there were no time lag before iron was produced, then the effects of iron production would mask the other two reactions making it very difficult to determine their rate constants. At low gas flow rates, as used in the present work, mass-transfer resistance is relatively significant in the overall reduction rate with the result that small variations in rate constants produce even smaller variation in the predicted reduction rate. Thus the reaction rate is not highly sensitive to the rate constants. Conversely, small changes in reaction rate will significantly affect the values of fitted rate constants.

Comparisons among the values given in Table III show that the average values of k_1, k_2 and b obtained from the consecutive reaction are in reasonable agreement with those determined for the single reactions. However, the values for the single reactions are probably more reliable since there were few data points below 30 pct reduction for the consecutive reaction, to which the model was fitted.

From the average values of k_3 at each temperature an activation energy of 27.7 kcal/g-mol was determined for the wüstite-to-iron reaction. This activation energy may be compared with a value of 24.5 kcal/g-mol reported by Scrivner[18] for the reduction of dense wüstite (ϵ^0 = 0.15 to 0.20) to iron by CO at 775 to 925°C.

When evaluated in terms of predictions of fractional reduction the effect of non-reproducibility of the fitted rate constants and sintering exponents is not a serious one. Fig. 12 compares the predicted fractional reduction using the average values of k_1, a, k_2, b, k_3 and c to the individually fitted curve for Run 140 at 800°C. This particular run was chosen because the individual value of k_3 had the largest deviation from average k_3. It is noted that the two curves are very close during the first 30 pct of reduction and that the predicted values of fractional reduction differ no more than 8 pct.

Table III. Average Rate Constants and Sintering Exponents

	750°C (1023 K)	775°C (1048 K)	800°C (1073 K)	Activation Energy kcal/g-mole (kJ/mole)
$k_1 \times 10^4$, cm/s				
Single rxn	0.916(± 50%)*	1.257(± 30%)	1.585(± 50%)	23.9 (100)
Consecutive rxn	0.893(± 40%)	1.086(± 40%)	1.300(± 70%)	16.5 (69.0)
a				
Single rxn	1.17	1.40	1.72	
Consecutive rxn	1.17	1.40	1.72	
$k_2 \times 10^4$, cm/s				
Single rxn	2.96(± 15%)	3.66(± 30%)	4.21(± 20%)	15.4 (64.4)
Consecutive rxn	2.35(± 50%)	3.39(± 45%)	4.18(± 30%)	18.7 (78.2)
b				
Single rxn	1.70	1.80	1.90	
Consecutive rxn	1.75	1.71	1.56	
$k_3 \times 10^4$, cm/s				
Consecutive rxn	2.63(± 10%)	3.50(± 40%)	4.97(± 45%)	27.7 (116)
c				
Consecutive rxn	1.10	1.30	2.00	

*Figures in parentheses are percentage variations of the fitted values from the average.

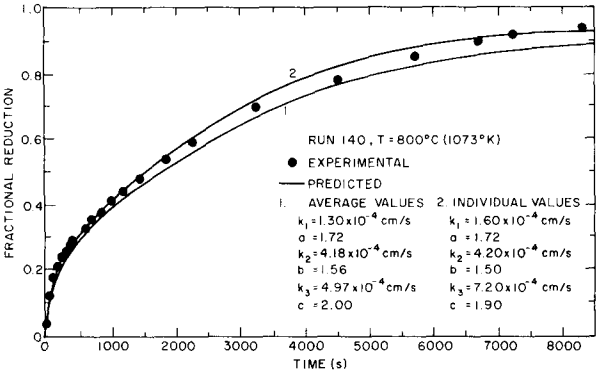

Fig. 12—Comparison of predicted curves for the reduction of hematite to iron at 800°C using average and individually fitted values of rate constants and sintering exponents.

CONCLUSIONS

The reduction of porous iron oxides (hematite, magnetite and wüstite) occurs non-topochemically, the degree of non-topochemical reduction decreasing with increasing temperature.

As temperature increases, the extent of sintering increases and the swelling of reduced iron decreases. The surface area of a particle undergoing reduction decreases continuously, independent of overall changes in particle size. The rate of decrease of surface area with fractional reduction increases as temperature increases.

A non-topochemical model is proposed, which a) allows particle size to change during reduction; b) includes local changes in void fraction, effective diffusivity, and reacting surface area; c) allows more than one reaction to occur in any region; d) reduces to the topochemical or homogeneous case when diffusion or chemical resistance, respectively, controls the reaction rate; and e) fits experimental data better than non-topochemical modesl proposed by others.

The reaction-rate constant of the wüstite-iron reaction is greater than that of the magnetite-wüstite reaction, which is greater than that of the hematite-magnetite reaction at any given temperature. The activation energies determined for each of the reduction reactions lie within the range of previously reported activation energies.

The reacting surface area can be related to the initial reactant surface area and the fraction of reactant remaining raised to a power called the sintering exponent, which is a measure of the degree of microscopic sintering occurring within a particle. The sintering exponent for each of the three reduction reactions increases as temperature increases.

ACKNOWLEDGMENTS

The authors are grateful to the U. S. Bureau of

Mines and the American Iron and Steel Institute for their financial support.

NOMENCLATURE

a	Sintering exponent for hematite-magnetite reaction
b	Sintering exponent for magnetite-wüstite reaction
c	Sintering exponent for wüstite-iron reaction
c_i	Moles of gas i/cm^3 of gas (10^6 mol.m^{-3})
c'_j	Moles of solid j/cm^3 of particle
c^0_j	Initial concentration of solid j, mol/cm^3 of particle
D_i	Effective diffusivity of i, cm^2/s (10^{-4} m^2.s^{-1})
$\mathfrak{D}_{CO\text{-}CO_2}$	Binary diffusion coefficient of CO in CO_2, cm^2/s
k_G	Mass transfer coefficient of CO, cm/s (10^{-2} m.s^{-1})
k_1, k_{-1}	Rate constants for hematite-magnetite reaction, cm/s
k_2, k_{-2}	Rate constants for magnetite-wüstite reaction, cm/s
k_3, k_{-3}	Rate constants for wüstite-iron reaction, cm/s
K_2	Equilibrium constant for magnetite-wüstite reaction, k_2/k_{-2}
K_3	Equilibrium constant for wüstite-iron reaction, k_3/k_{-3}
m^0	Initial mass of particle, g (10^{-3} kg)
M_j	Molecular weight of solid species j
p	Total pressure, atm (1.013×10^5 Pa)
p_i	Partial pressure of gas i, atm
p_i^b	Partial pressure of i in bulk gas phase, atm
q	Radial sintering factor for magnetite-wüstite reaction, Eq. [24]
R	Universal gas constant, 82.06 atm cm^3/mol K (8.314 J mol^{-1} K^{-1})
r	Radial position, cm (10^{-2} m)
r_0	Particle radius, cm
r_0^0	Initial radius of particle, cm
r_0^∞	Final radius of particle, cm
r_j^0	Radius of particle of pure j, cm
R'_i	Generation rate of gas i per unit volume of particle, mol/cm^3 s (10^6 mol.m^{-3}.s^{-1})
R'_j	Generation rate of solid j per unit volume of particle, mol/s cm^3
S_j	Surface area of solid reactant j per unit volume of particle, cm^{-1} (10^2 m^{-1})
S_j^0	Initial surface area of pure solid reactant j per unit volume of particle, cm^{-1}
s_j^0	Initial surface area of pure solid reactant j per unit mass, m^2/g (10^3 m^2.kg^{-1})
t	Time, s
T	Temperature, K
u	Velocity of solid, cm/s (10^{-2} m.s^{-1})
v^*	Molar average velocity of gas, cm/s
x	Stoichiometric factor for variable wüstite, Fe_xO, composition
X_j	Fraction of iron atoms as component j locally
$\overline{X}_j$	Average fraction of iron atoms as j

Greek

ϵ	Local void fraction of solid
ϵ^0	Initial void fraction of particle
ρ_j	Density of pure solid component j, g/cm^3 (10^3 Kg.m^{-3})

Subscript j

h	hematite
m	magnetite
w	wüstite
Fe	iron

REFERENCES

1. R. H. Spitzer, F. S. Manning, and W. O. Philbrook: *Trans. TMS-AIME*, 1966, vol. 236, pp. 726-42.
2. R. H. Spitzer, F. S. Manning, and W. O. Philbrook: *ibid.*, 1966, vol. 236, pp. 1715-24.
3. R. H. Spitzer, F. S. Manning, and W. O. Philbrook: *ibid.*, 1968, vol. 242, pp. 618-25.
4. W. D. Ahner and J. Feinman: *AIChE J.*, 1964, vol. 10, pp. 652-55.
5. W. J. Helfrich and C. L. Sollenberger: *Trans. TMS-AIME*, 1961, vol. 220, pp. 485-90.
6. J. P. Hansen, G. Bitsianes, and T. L. Joseph: *Blast Furnace, Coke Oven and Raw Mater. Proc., AIME*, 1960, vol. 19, pp. 185-99.
7. J. O. Edström: *J. Iron Steel Inst.*, 1953, vol. 175, pp. 289-304.
8. J. O. Edström: *Jernkontorets Ann.*, 1957, vol. 141, pp. 809-36.
9. E. T. Turkdogan and J. V. Vinters: *Met. Trans.*, 1971, vol. 2, pp. 3175-88.
10. I. H. Bowen and C. K. Cheng: *Chem. Eng. Sci.*, 1969, vol. 24, pp. 1829-31.
11. M. Ishida and C. Y. Wen: *AIChE J.*, 1968, vol. 14, pp. 311-17.
12. M. Ishida and C. Y. Wen: *Chem. Eng. Sci.*, 1968, vol. 23, pp. 125-37.
13. J. Szekely and J. W. Evans: *Met. Trans.*, 1971, vol. 2, pp. 1691-98.
14. J. Szekely and J. W. Evans: *ibid.*, 1971, vol. 2, pp. 1699-1710.
15. W. E. Ranz: *Chem. Eng. Progr.*, 1952, vol. 48, pp. 247-53.
16. R. A. Newby: Ph.D. Thesis, Carnegie-Mellon University, Pittsburgh, Pa., 1971.
17. C. Y. Wen: *Ind. Eng. Chem.*, 1968, vol. 60, no. 9, pp. 34-54.
18. N. C. Scrivner: Ph.D. Thesis, Carnegie-Mellon University, Pittsburgh, Pa., 1972.